Available online at www.sciencedirect.com

SciVerse ScienceDirect

Ceramics International 38 (2012) 5133–5138

CERAMICS INTERNATIONAL

www.elsevier.com/locate/ceramint

Effect of $FeAl_3$ on properties of (W,Ti)C–$FeAl_3$ hard materials consolidated by a pulsed current activated sintering method

In-Jin Shon [a,*], Kwon-Il Na [a], In-Yong Ko [a], Jung-Mann Doh [b], Jin-Kook Yoon [b]

[a] *Division of Advanced Materials Engineering and the Research Center of Industrial Technology, Engineering College, Chonbuk National University, 561-756, Republic of Korea*

[b] *Advanced Functional Materials Research Center, Korea Institute of Science and Technology, PO Box 131, Cheongryang, Seoul 130-650, Republic of Korea*

Received 28 September 2011; received in revised form 29 February 2012; accepted 6 March 2012
Available online 14 March 2012

Abstract

Using a pulsed current activated sintering (PCAS) method, the densification of (W,Ti)C and (W,Ti)C–$FeAl_3$ hard materials was accomplished within 3 min. The advantage of this process is not only rapid densification to near theoretical density, but also prevention of grain growth in nanostructured materials. Highly dense (W,Ti)C and (W,Ti)C–$FeAl_3$ with a relative density up to 99% were obtained within 3 min by PCAS under a pressure of 80 MPa. The average grain size of the (W,Ti)C was less than 100 nm. Hardness and fracture toughness of the dense (W,Ti)C and (W,Ti)C–$FeAl_3$ produced by PCAS were also investigated. The fracture toughness and hardness values of (W,Ti)C, (W,Ti)C–5 vol.% $FeAl_3$, and (W,Ti)C–10 vol.% $FeAl_3$ consolidated by PCAS were 7.5 MPa $m^{1/2}$ and 2650 kg/mm^2, 10.5 MPa $m^{1/2}$ and 2480 kg/mm^2, 11 MPa $m^{1/2}$ and 2300 kg/mm^2, respectively.

Keywords: A. Sintering; C. Hardness; Fracture toughness; Nanomaterials

1. Introduction

(W,Ti)C has a high melting point and high hardness. In this regard, the transition metal carbide is primarily used in cutting tools and as an abrasive material as a single phase or in composite structures. In the case of cemented (W,Ti)C, Co or Ni is added as a binder for the formation of composite structures. However, the high cost of Co or Ni and the low corrosion resistance of the (W,Ti)C–Co or (W,Ti)C–Ni cement have generated recent interest in alternative binder phases [1–4]. It has been reported that iron aluminides show a higher oxidation resistance, a higher hardness and are less expensive materials compared to Co and Ni [5].

Improvement in mechanical properties and stability of cemented carbides has been achieved through microstructural changes such as grain size refinement [6,7]. However, the use of conventional methods to consolidate nanopowders often leads to grain growth. Grain growth can be minimized by sintering at lower temperatures and for shorter times. In this regard, the pulsed current activated sintering (FCAS) technique has been shown to be effective in the sintering of nanostructured materials in very short times (within 1 min) [8,9].

We present here the results of the sintering of (W,Ti)C and (W,Ti)C–$FeAl_3$ composites by a rapid sintering process, pulsed current activated sintering, with simultaneous application of pulsed current and high pressure. The goal of this study is to produce dense and nanocrystalline (W,Ti)C and (W,Ti)C–$FeAl_3$ hard materials in very short sintering times (<3 min). Also, we have investigated the effect of novel $FeAl_3$ binder on the mechanical properties of (W,Ti)C hard materials.

2. Experimental procedure

The (Ti,W)C powder with a grain size of <1 μm and 99% purity used in this research was supplied by H.C. Starck. $FeAl_3$ (<45 μm, 99.5% pure, Sejong Co.) was used as a binder material. Three various compositions of (W,Ti)C, (W,Ti)C–5 vol.% $FeAl_3$, and (W,Ti)C–10 vol.% $FeAl_3$ were investigated. The powder was first milled in a high-energy ball mill

* Corresponding author. Tel.: +82 63 270 2381; fax: +82 63 270 2386.
E-mail addresses: ijshon@chonbuk.ac.kr, ijshon@jbnu.ac.kr (I.-J. Shon).

0272-8842/$36.00
doi:10.1016/j.ceramint.2012.03.017

(Pulverisette-5 planetary mill) at 250 rpm for 10 h. Tungsten carbide balls (9 mm in diameter) were used in sealed cylindrical stainless steel vials under an argon atmosphere. The weight ratio of balls-to-powder was 30:1. Milling resulted in a significant reduction in grain size. Grain size of the (W,Ti)C was calculated from the full width at half-maximum (FWHM) of the diffraction peak using the formula suggested by Suryanarayana and Grant Norton [10]:

$$B_r(B_{crystalline} + B_{strain})\cos\theta = k\frac{\lambda}{L} + \eta\sin\theta \quad (1)$$

where B_r is the full width at half-maximum (FWHM) of the diffraction peak after instrument correction; $B_{crystalline}$ and B_{strain} are the FWHM values caused by small grain size and internal stress, respectively; k is a constant (with a value of 0.9); λ is the wavelength of the X-ray radiation; L and η are grain size and internal strain, respectively; and θ is the Bragg angle. Parameters B and B_r follow Cauchy's form with the relationship: $B = B_r + B_s$, where B and B_s are the FWHM values of the broadened Bragg peaks and the standard sample Bragg peaks, respectively.

The milled powders were placed in a graphite die (outside diameter, 45 mm; inside diameter, 20 mm; height, 40 mm) and were then introduced into a pulsed-current activated sintering (PCAS) system manufactured by Eltek Co. in the Republic of Korea. A schematic diagram of this system is shown in Fig. 1. The PCAS apparatus includes an 18 V, 2800 A DC power supply (which provides a pulsed current with a 20 μs on time and a 10 μs off time through the sample and die) and a uniaxial press with a maximum load of 50 kN. The system was evacuated before analysis, and a uniaxial pressure of 80 MPa was applied. A pulsed DC current was then activated and maintained until the densification rate was negligible, as indicated by the observed shrinkage of the sample. Sample shrinkage was measured in real time using a linear gauge to measure vertical displacement. Temperatures were measured using a pyrometer focused on the surface of the graphite die. A temperature gradient from the surface to the center of the sample is dependent on the heating rate, the electrical and thermal conductivities of the compact, and its relative density. The process heating rates were approximately 600 K min^{-1}. At the end of the process, the current was turned off, and the sample was allowed to cool to room temperature. The entire process of densification using the PCAS technique consists of four major control stages of chamber evacuation, pressure application, power application, and cool down. The process was carried out under a vacuum of 5.33 Pa.

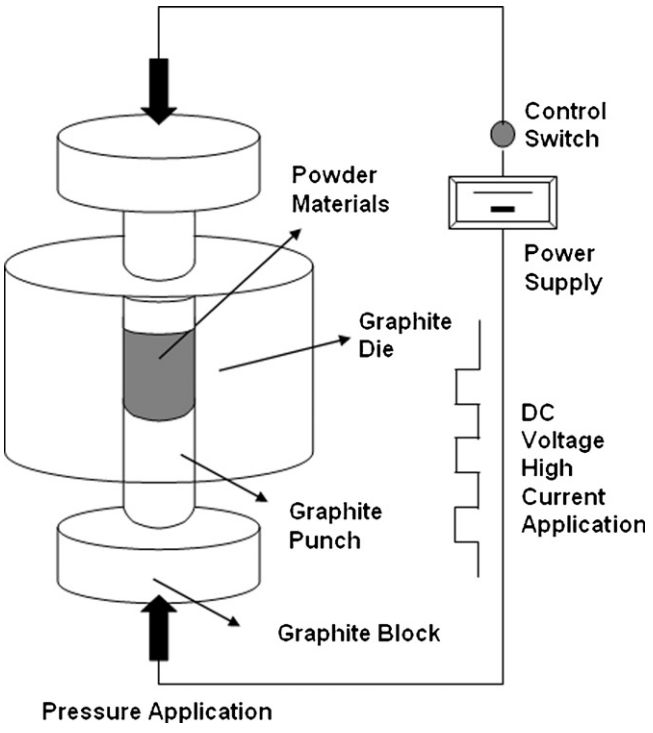

Fig. 1. Schematic diagram of the apparatus for pulsed current activated sintering (PCAS).

The relative densities of the sintered samples were measured using the Archimedes method. Microstructural information was obtained from the product samples, which had been polished and etched using Murakami's reagent (10 g potassium ferricyanide, 10 g sodium hydroxide, and 100 ml water) for 1–2 min at room temperature. Compositional and microstructural analyses of the products were carried out through X-ray diffraction (XRD), scanning electron microscopy (SEM) with energy dispersive X-ray spectroscopy (EDS), and field-emission scanning electron microscopy (FE-SEM). Vickers hardness was measured by performing indentations at a load of 10 kg_f with a dwell time of 15 s.

3. Results and discussion

SEM images of (Ti,W)C, (W,Ti)C–5 vol.% $FeAl_3$, and (W,Ti)C–10 vol.% $FeAl_3$ powders milled for 10 h are shown in Fig. 2. The (W,Ti)C powder has a round grain shape and became more refined with milling time. Fig. 3 shows X-ray diffraction patterns of the (W,Ti)C, (W,Ti)C–5 vol.% $FeAl_3$, and (W,Ti)C–10 vol.% $FeAl_3$ powders after milling for 10 h. (W,Ti)C and $FeAl_3$ peaks were detected in the (W,Ti)C–$FeAl_3$ powders. The average grain size of the (W,Ti)C milled for 10 h and calculated by the formula suggested by Suryanarayana and Grant Norton was about 20 nm.

The variations of shrinkage and temperature with heating time during the sintering of (W,Ti)C, (W,Ti)C–5 vol.% $FeAl_3$, and (W,Ti)C–10 vol.% $FeAl_3$ powders by PCAS under 80 MPa pressure and a pulsed DC current of 2800 A are shown in Fig. 4. In all cases, the application of the pulsed current resulted in shrinkage due to consolidation. The temperatures of shrinkage initiation and abrupt shrinkage were reduced remarkably by the addition of $FeAl_3$. As such, it is expected that $FeAl_3$ is molten during the sintering process. The main densification mechanisms for this are the rearrangement of carbide particles, enhancement in the diffusion, and viscous flow of the binder [11].

Fig. 5 shows the XRD patterns of (W,Ti)C, (W,Ti)C–5 vol.% $FeAl_3$, and (W,Ti)C–10 vol.% $FeAl_3$ after sintering by the PCAS method. In all cases, only (W,Ti)C peaks are detected; heavier contaminants, such as iron from the milling container,

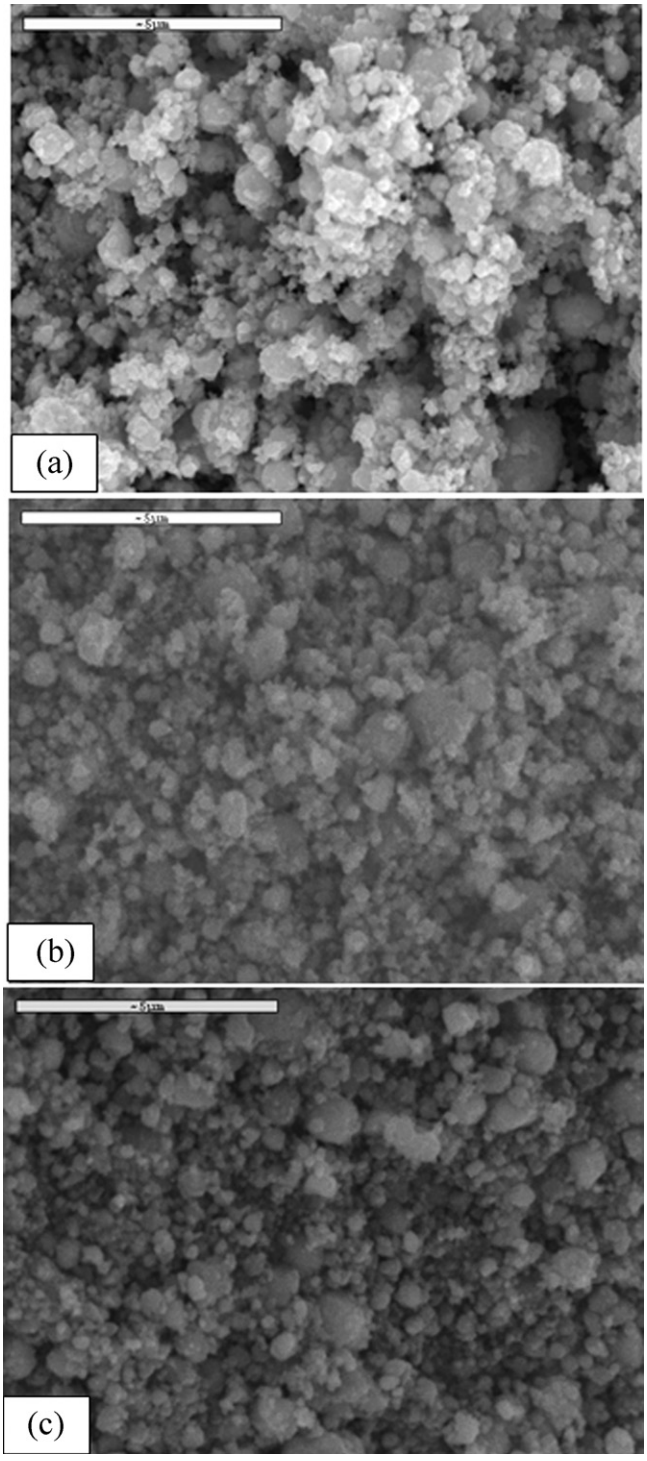

Fig. 2. Scanning electron microscope images of powders milled for 10 h: (a) (W,Ti)C, (b) (W,Ti)C–5 vol.% $FeAl_3$, and (c) (W,Ti)C–10 vol.% $FeAl_3$.

were not detected. A plot of $B_r(B_{crystalline} + B_{strain})\cos\theta$ versus $\sin\theta$ in Suryanarayana and Grant Norton's formula is shown in Fig. 6. The average grain sizes of the (Ti,W)C calculated from the XRD data are about 60, 40, and 50 nm for samples with (W,Ti)C, (W,Ti)C–5 vol.% $FeAl_3$, and (W,Ti)C–10 vol.% $FeAl_3$, respectively. FE-SEM images of the etched samples after being sintered up to about 1300 °C are shown in Fig. 7. From the figure, it is apparent that the grain size of (Ti,W)C

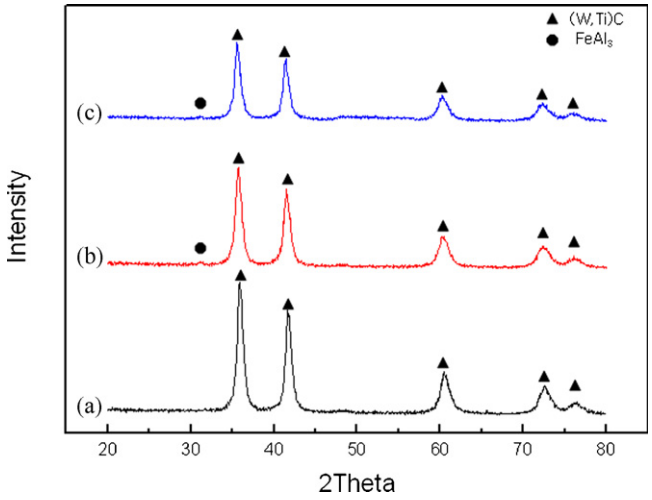

Fig. 3. X-ray diffraction patterns of powders milled for 10 h: (a) (W,Ti)C, (b) (W,Ti)C–5 vol.% $FeAl_3$, and (c) (W,Ti)C–10 vol.% $FeAl_3$.

consists of nanocrystallites. Thus, the average grain size of the sintered (Ti,W)C is not much larger than that of the initial powder, indicating the absence of grain growth during sintering. This retention of grain size is attributed to the high heating rate and the relatively short term exposure of the powders to high temperature. The relative densities of (W,Ti)C, (W,Ti)C–5 vol.% $FeAl_3$, and (W,Ti)C–10 vol.% $FeAl_3$ were approximately 99%.

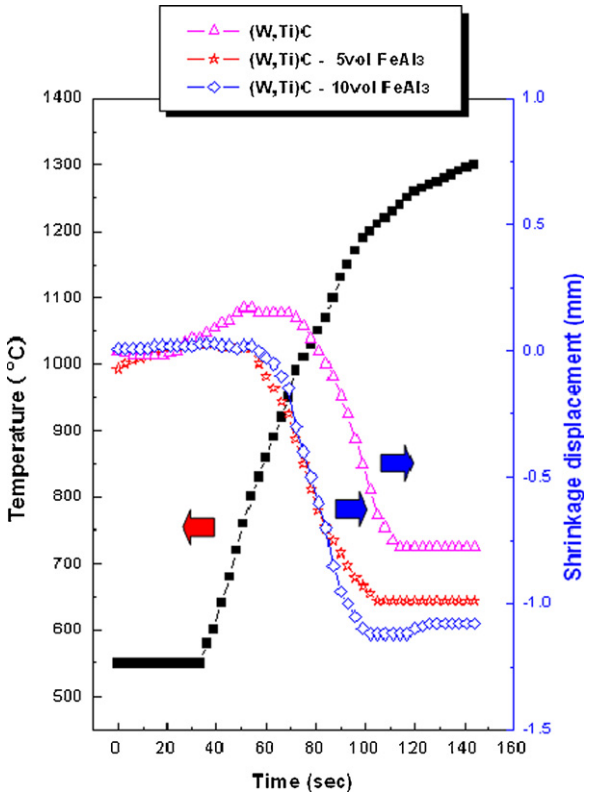

Fig. 4. Variations of temperature and shrinkage displacement with heating time during the sintering of (W,Ti)C, (W,Ti)C–5 vol.% $FeAl_3$, and (W,Ti)C–10 vol.% $FeAl_3$ hard materials by PCAS.

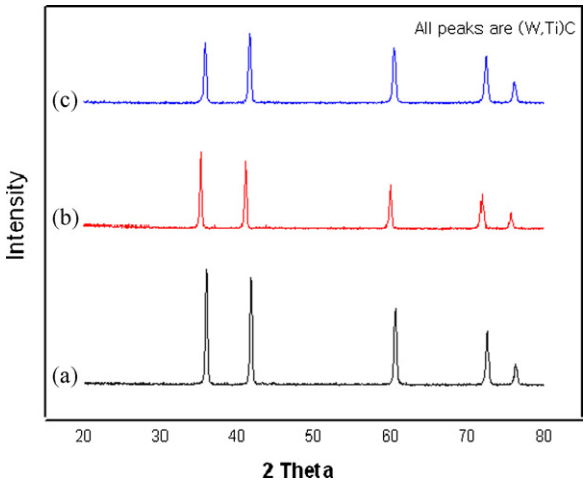

Fig. 5. XRD patterns of (a) (W,Ti)C, (b) (W,Ti)C–5 vol.% $FeAl_3$, and (c) (W,Ti)C–10 vol.% $FeAl_3$ hard materials produced by PCAS.

The role of the current in sintering and/or synthesis has been the focus of several attempts to explain the observed sintering enhancement and the improved characteristics of the products. The role played by the current has been variously interpreted. Explanations include fast heating due to Joule heating at contacts points, the presence of plasma in pores separating powder particles, and the intrinsic contribution of the current to mass transport [12–15].

Vickers hardness measurements were performed on polished sections of the (W,Ti)C, (W,Ti)C–5 vol.% $FeAl_3$, and (W,Ti)C–10 vol.% $FeAl_3$ samples using a 10 kg load and 15 s dwell time. Indentations with large loads produced median cracks around the indentation. The lengths of these cracks permit estimation of the fracture toughness of the materials by means of the expression [16]:

$$K_{IC} = 0.204\left(\frac{c}{a}\right)^{-3/2} \cdot H_v \cdot a^{1/2} \quad (2)$$

where c is the trace length of the crack measured from the center of the indentation, a is one-half of the average length of the two indent diagonals, and H_v is the hardness.

The Vickers hardnesses and the fracture toughnesses of the (W,Ti)C, (W,Ti)C–5 vol.% $FeAl_3$, and (W,Ti)C–10 vol.% $FeAl_3$ samples were 2660, 2480, 2300 kg/mm^2, and 7.5, 10.5, 11 MPa m$^{1/2}$, respectively. These values represent the average of five measurements. Vickers hardness indentations in the (W,Ti)C, (W,Ti)C–5 vol.% $FeAl_3$, and (W,Ti)C–10 vol.% $FeAl_3$ samples are shown in Fig. 8, which shows that one to three additional cracks were typically observed to propagate radially from the indentation. A comparison of the hardness and fracture toughness values obtained in this study with those reported by others is provided in Table 1 [17]. In one of the reported studies [17], WC–10Co and WC–10Ni were consolidated at 1250 °C by high-frequency induction heated sintering. Referring to Table 1, it is seen that addition of $FeAl_3$ to (W,Ti)C significantly improves the fracture toughness of cemented (W,Ti)C without greatly decreasing the hardness. Also, comparing this investigation of (W,Ti)C–5$FeAl_3$, and

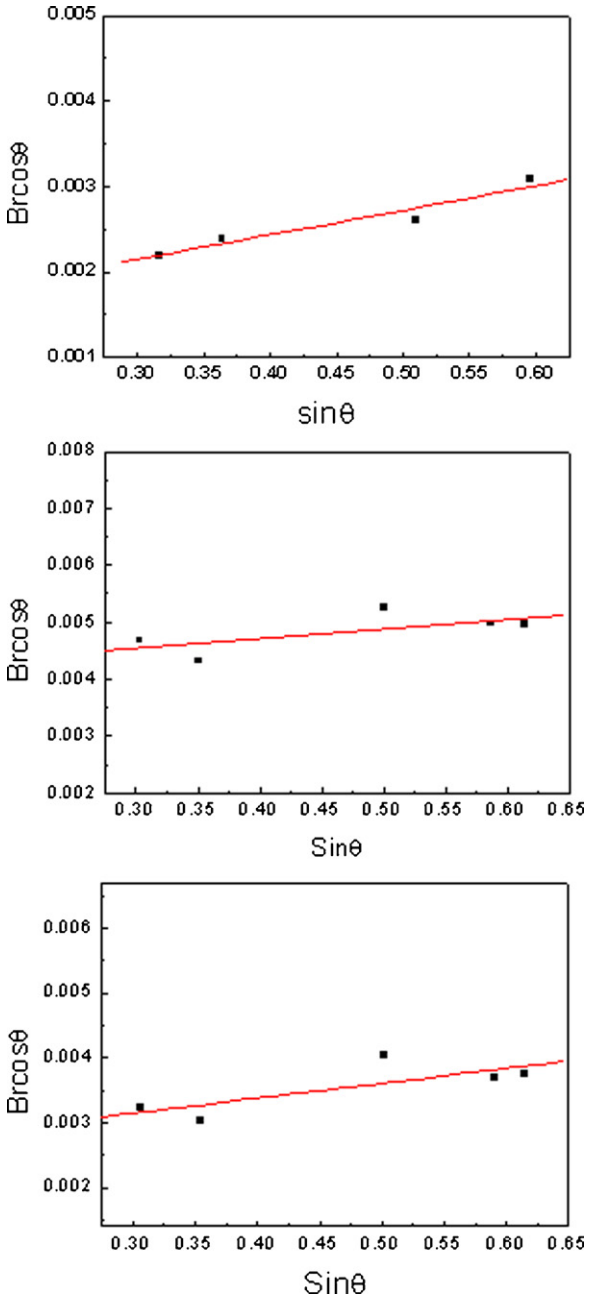

Fig. 6. Plot of $B_r(B_{crystalline} + B_{strain})\cos\theta$ versus $\sin\theta$ for (Ti,W)C in (a) (W,Ti)C, (b) (W,Ti)C–5 vol.% $FeAl_3$, and (c) (W,Ti)C–10 vol.% $FeAl_3$ hard materials sintered from milled powders.

(W,Ti)C–10$FeAl_3$ with a study of WC–10Co and WC–10Ni [17], there is little difference in fracture toughness, but hardness in the present study is higher than that in the previous study [17].

4. Summary

Using pulsed current activated sintering (PCAS), the rapid consolidation of (W,Ti)C, (W,Ti)C–5 vol.% $FeAl_3$, and (W,Ti)C–10 vol.% $FeAl_3$ hard materials was accomplished. Nearly fully dense (W,Ti)C and (W,Ti)C–$FeAl_3$ composites could be obtained within 3 min. The densification temperature

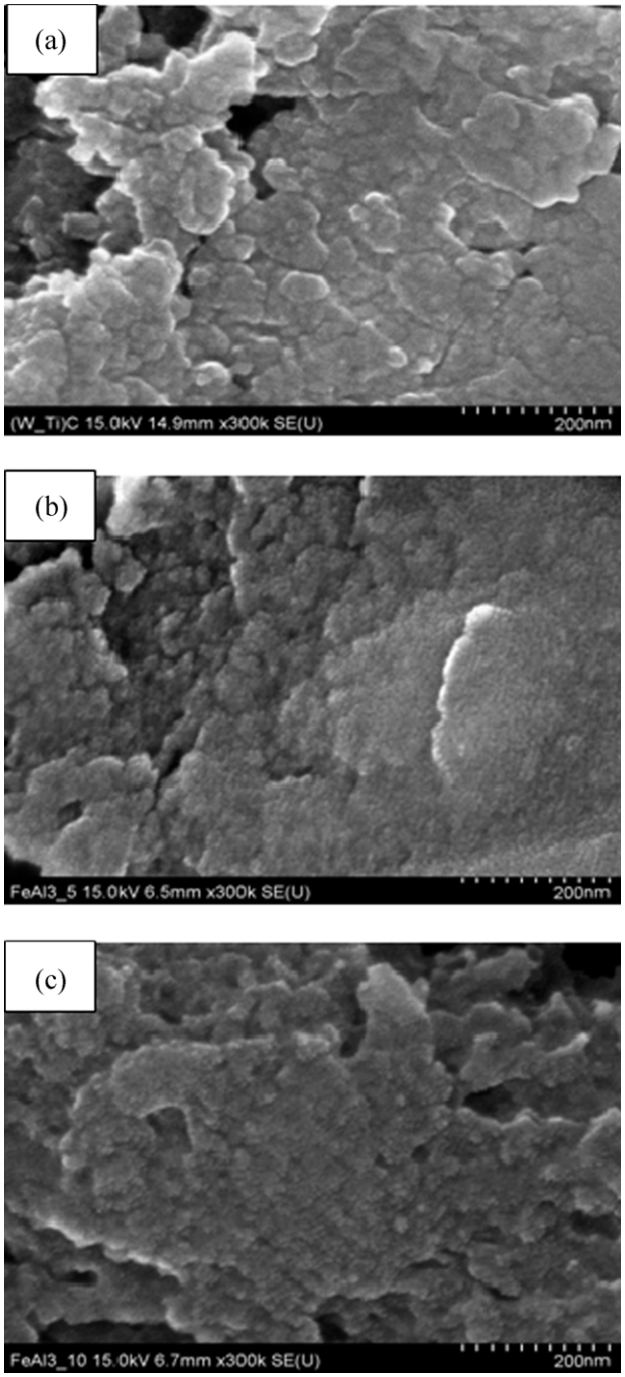

Fig. 7. FE-SEM images of (a) (W,Ti)C, (b) (W,Ti)C–5 vol.% $FeAl_3$, and (c) (W,Ti)C–10 vol.% $FeAl_3$ hard materials produced by PCAS.

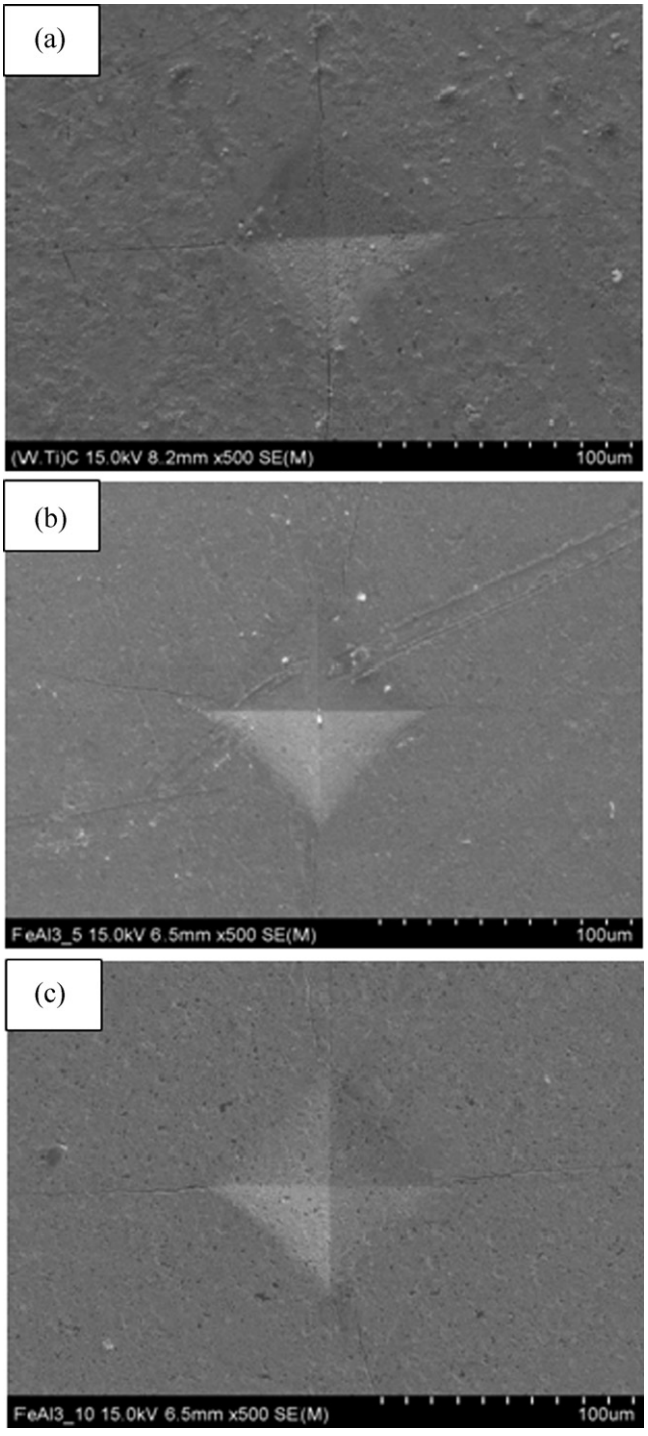

Fig. 8. Vickers hardness indentation in (a) (W,Ti)C, (b) (W,Ti)C–5 vol.% $FeAl_3$, and (c) (W,Ti)C–10 vol.% $FeAl_3$ hard materials produced by PCAS.

Table 1
Comparison of mechanical properties of (W,Ti)C, (W,Ti)C–5 vol.% $FeAl_3$, and (W,Ti)C–10 vol.% $FeAl_3$ in this work with previously reported values.

Ref.	Binder content (vol%)	Relative density (%)	Grain size (nm)	H_v (kg/mm^2)	K_{IC} (MPa m$^{1/2}$)
[17]	10Co	98.2	450	1776	10.6
[17]	10Ni	99.1	490	1750	11.1
This study	0	99	60	2650	7.5
	5FeAl3	99	40	2480	10.5
	10FeAl3	99	50	2300	11

of (W,Ti)C was reduced remarkably by the addition of $FeAl_3$. The grain sizes of (W,Ti)C in (W,Ti)C, (W,Ti)C–5 vol.% $FeAl_3$, and (W,Ti)C–10 vol.% $FeAl_3$ hard materials were about 60 nm, 40 nm and 50 nm, respectively. The fracture toughness and hardness values of (W,Ti)C, (W,Ti)C–5 vol.% $FeAl_3$, and (W,Ti)C–10 vol.% $FeAl_3$ consolidated by PCAS with a pressure of 80 MPa and a pulsed DC current of 2800 A were 7.5 MPa $m^{1/2}$ and 2650 kg/mm^2, 10.5 MPa $m^{1/2}$ and 2480 kg/mm^2, 11 MPa $m^{1/2}$ and 2300 kg/mm^2, respectively.

References

[1] S. Imasato, K. Tokumoto, T. Kitada, S. Sakaguchi, Properties of ultra-fine grain binderless cemented carbide RCCFN, Int. J. Refract. Met. Hard Mater. 13 (5) (1995) 305–312.

[2] E.A. Almond, B. Roebuck, Identification of optimum binder phase compositions for improved WC hard metals, Mater. Sci. Eng. A 105/106 (1988) 237–248.

[3] G. Gille, J. Bredthauer, B. Gries, B. Mende, Advanced and new grades of WC and binder powder-their properties and application, Int. J. Refract. Met. Hard Mater. 18 (2,3) (2000) 87–102.

[4] P. Goeuriot, F. Thevenot, Boron as sintering assitive in cemented WC–Co (or Ni) alloys, Ceram. Int. 13 (2) (1987) 99–103.

[5] Z.G. Zhang, F. Gesmundo, P.Y. Hou, Y. Niu, Criteria for the formation of protective Al_2O_3 scale on Fe–Al and Fe–Cr–Al alloys, Corros. Sci. 48 (2006) 741–765.

[6] H. Gleiter, Nanocrystalline materials, Prog. Mater. Sci. 33 (4) (1989) 223–315.

[7] G.E. Fougere, J.R. Weertman, R.W. Siegel, S. Kim, Grain-size dependent hardening and softening of nanocrystalline Cu and Pd, Scripta Metall. Mater. 26 (12) (1992) 1879–1883.

[8] H.C. Kim, I.J. Shon, Z.A. Munir, Rapid sintering of ultra-fine WC–10 wt% Co by high-frequency induction heating, J. Mater. Sci. 40 (2005) 2849–2854.

[9] H.C. Kim, D.Y. Oh, I.J. Shon, Sintering of nanophase WC–15 vol.% Co hard metals by rapid sintering process, Int. J. Refract. Met. Hard Mater. 22 (4,5) (2004) 197–203.

[10] C. Suryanarayana, M. Grant Norton, X-ray Diffraction A Practical Approach, Plenum Press, New York, 1998.

[11] G.S. Upadhyaya, Materials science of cemented carbides – an overview, Mater. Des. 22 (6) (2001) 483–489.

[12] Z. Shen, M. Johnsson, Z. Zhao, M. Nygren, Spark plasma sintering of alumina, J. Am. Ceram. Soc. 85 (2002) 1921–1927.

[13] J.E. Garay, U. Anselmi-Tamburini, Z.A. Munir, S.C. Glade, P. Asoka-Kumar, Electric current enhanced defect mobility in Ni_3Ti intermetallics, Appl. Phys. Lett. 85 (2004) 573–575.

[14] J.R. Friedman, J.E. Garay, U. Anselmi-Tamburini, Z.A. Munir, Modified interfacial reactions in Ag–Zn multilayers under the influence of high DC currents, Intermetallics 12 (2004) 589–597.

[15] J.E. Garay, U. Anselmi-Tamburini, Z.A. Munir, Enhanced growth of intermetallic phases in the Ni–Ti system by current effects, Acta Mater. 51 (2003) 4487–4495.

[16] K. Niihara, R. Morena, D.P.H. Hasselman, Evaluation of KIC of brittle solids by the indentation method with low crack-to-indent ratios, J. Mater. Sci. Lett. 1 (1982) 12–16.

[17] I.J. Shon, I.K. Jeong, I.Y. Ko, J.M. Doh, K.D. Woo, Sintering behavior and mechanical properties of WC–10Co, WC–10Ni and WC–10Fe hard materials produced by high-frequency induction heated sintering, Ceram. Int. 35 (2009) 339–344.